Molecular Plant
Research article

CellPress
Partner Journal

Submergence promotes auxin-induced callus formation through ethylene-mediated post-transcriptional control of auxin receptors

Seung Yong Shin[1,2], Yuri Choi[3], Sang-Gyu Kim[3], Su-Jin Park[1,4], Ji-Sun Park[1], Ki-Beom Moon[1], Hyun-Soon Kim[1,4], Jae Heung Jeon[1], Hye Sun Cho[1,4] and Hyo-Jun Lee[1,2,5,*]

[1]Plant Systems Engineering Research Center, Korea Research Institute of Bioscience and Biotechnology, Daejeon 34141, Korea

[2]Department of Functional Genomics, KRIBB School of Bioscience, University of Science and Technology, Daejeon 34113, Korea

[3]Department of Biological Sciences, Korea Advanced Institute of Science and Technology, Daejeon 34141, Korea

[4]Department of Biosystems and Bioengineering, KRIBB School of Biotechnology, University of Science and Technology, Daejeon 34113, Korea

[5]Department of Biological Sciences, Sungkyunkwan University, Suwon 16419, Korea

***Correspondence: Hyo-Jun Lee (hyojunlee@kribb.re.kr)**

https://doi.org/10.1016/j.molp.2022.11.001

ABSTRACT

Plant cells in damaged tissue can be reprogrammed to acquire pluripotency and induce callus formation. However, in the aboveground organs of many species, somatic cells that are distal to the wound site become less sensitive to auxin-induced callus formation, suggesting the existence of repressive regulatory mechanisms that are largely unknown. Here we reveal that submergence-induced ethylene signals promote callus formation by releasing post-transcriptional silencing of auxin receptor transcripts in non-wounded regions. We determined that short-term submergence of intact seedlings induces auxin-mediated cell dedifferentiation across the entirety of *Arabidopsis thaliana* explants. The *constitutive triple response 1-1* (*ctr1-1*) mutation induced callus formation in explants without submergence, suggesting that ethylene facilitates cell dedifferentiation. We show that ETHYLENE-INSENSITIVE 2 (EIN2) post-transcriptionally regulates the abundance of transcripts for auxin receptor genes by facilitating microRNA393 degradation. Submergence-induced calli in non-wounded regions were suitable for shoot regeneration, similar to those near the wound site. We also observed submergence-promoted callus formation in Chinese cabbage (*Brassica rapa*), indicating that this may be a conserved mechanism in other species. Our study identifies previously unknown regulatory mechanisms by which ethylene promotes cell dedifferentiation and provides a new approach for boosting callus induction efficiency in shoot explants.

Key words: cell dedifferentiation, auxin signaling, ethylene, callus formation, EIN2

Shin S.Y., Choi Y., Kim S.-G., Park S.-J., Park J.-S., Moon K.-B., Kim H.-S., Jeon J.H., Cho H.S., and Lee H.-J. (2022). Submergence promotes auxin-induced callus formation through ethylene-mediated post-transcriptional control of auxin receptors. Mol. Plant. **15**, 1947–1961.

INTRODUCTION

Plant cells can reprogram their identity to acquire pluripotency and regenerate new organs (Lee and Seo, 2018; Ikeuchi et al., 2019). Incubating detached tissue on auxin-rich callus-inducing medium (CIM) induces the transition of somatic cells into an unorganized, pluripotent tissue called a callus (Lee and Seo, 2018; Ikeuchi et al., 2019). When leaf explants are used for callus formation, cellular dedifferentiation occurs rapidly near the wound site even though the entire explant is in contact with the medium (Xu et al., 2018b; Lee et al., 2018). This observation suggests that cellular identity reprogramming is less active farther from the wound site. However, the regulatory mechanisms repressing cell dedifferentiation in distal regions of the explants remain elusive.

Auxin-induced callus formation and lateral root formation follow similar developmental programs (Lee and Seo, 2018; Ikeuchi et al., 2019). Because auxin plays a critical role in lateral root development, genes involved in auxin-mediated root organogenesis are also involved in callus formation. In *Arabidopsis thaliana* (hereafter referred to as *Arabidopsis*), expression of *LATERAL*

Published by the Molecular Plant Shanghai Editorial Office in association with Cell Press, an imprint of Elsevier Inc., on behalf of CSPB and CEMPS, CAS.

ORGAN BOUNDARIES DOMAIN (*LBD*) genes, including *LBD16*, is rapidly induced during callus formation on CIM (Fan et al., 2012; Xu et al., 2018a). Similar to root organogenesis, WUSCHEL-RELATED HOMEOBOX 11 (WOX11) and WOX12 are upstream regulators of *LBD*s, and expression of *WOX11* and *WOX12* is increased by auxin (Liu et al., 2014). LBD16 induces expression of *WOX5*, a gene involved in regulating root stem cell identity (Sarkar et al., 2007). Strong overexpression of *WOX11*, *LBD16*, *LBD17*, *LBD18*, or *LBD29* triggers callus formation (Fan et al., 2012; Liu et al., 2014), indicating that the WOX11/12-LBD-WOX5 signaling module is a key regulator of cell fate transitions. Wound-induced callus formation, however, is regulated by different molecular signaling pathways. Callus formation at the wound site is not suppressed in the *Arabidopsis* lateral root initiation mutant *solitary root* (Iwase et al., 2011), suggesting that lateral root developmental pathways are not involved. Instead of auxin signaling, cytokinin biosynthesis and WOUND-INDUCED DEDIFFERENTIATION 1 (WIND1)-mediated cytokinin signaling induce callus formation at wound sites (Iwase et al., 2011; Ikeuchi et al., 2017). Auxin-induced callus formation occurs in pericycle and pericycle-like cells, whereas wound-induced calli are not limited to specific cell types (Atta et al., 2009; Iwase et al., 2011).

Ethylene is a gaseous phytohormone that regulates a number of developmental processes and stress responses (Alonso et al., 1999; Stepanova and Alonso, 2009; Dolgikh et al., 2019). Ethylene signaling begins with perception of ethylene by endoplasmic reticulum-localized ethylene receptors (Schaller and Bleecker, 1995; Dolgikh et al., 2019; Binder, 2020). Ethylene binding to these receptors blocks their function, leading to inactivation of the serine-threonine protein kinase CONSTITUTIVE TRIPLE RESPONSE 1 (CTR1) (Dolgikh et al., 2019; Binder, 2020). Inactive CTR1 no longer phosphorylates the C-terminal domain of ETHYLENE-INSENSITIVE 2 (EIN2), which can then be cleaved and is released from the endoplasmic reticulum membrane. The C-terminal domain of EIN2 then translocates to the nucleus, where it activates EIN3 and EIN3-LIKE 1 (EIL1) transcription factors to induce expression of ethylene-responsive genes (Ju et al., 2012; Dolgikh et al., 2019). Ethylene is also involved in regulation of callus formation in plants. Inhibition of ethylene signaling increases callus production in maize (*Zea mays*) and rice (*Oryza sativa*) explants (Vain et al., 1990; Adkins et al., 1993), and the ethylene precursor 1-aminocyclopropane-1-carboxylic acid (ACC) stimulates callus formation in *Citrus* (Tadeo et al., 1995). These reports suggest that ethylene controls callus formation in several species. However, the molecular mechanisms by which ethylene signaling regulates cell fate transitions in explants are largely unknown.

Here we report that auxin-induced callus formation is suppressed in areas distal from the wound site but that ethylene releases this suppression in shoot explants. Activation of ethylene signaling by short-term submergence or the *ctr1-1* mutation induced auxin responses in the explants. We demonstrate that EIN2-mediated post-transcriptional regulation of auxin receptor genes is a key mechanism of callus formation. Our work reveals that short-term submergence and ethylene promote callus formation and, therefore, could be used to break dormancy in cell dedifferentiation and improve regeneration capacity during plant tissue culture.

RESULTS

Submergence promotes callus formation

In our previous study, we showed that short-term submergence inhibited plant wound responses mediated by jasmonic acid (JA) biosynthesis (Lee et al., 2020). Because wounding is a cue for cell fate transition (Chen et al., 2016; Ikeuchi et al., 2017), we hypothesized that submergence might affect callus formation in detached leaves as well. When *Arabidopsis* seedlings were submerged for 1 h before leaf detachment, callus formation occurred across the entire explant (i.e., not restricted to the wound site) after incubation on CIM (Figure 1A and 1B). The effects of submergence were not dependent on excision sites because explants from leaf blades and entire leaves (containing the petiole) produced calli across the entire tissue after submergence (Supplemental Figure 1A). However, root explants produced widespread calli under control and submergence conditions (Supplemental Figure 1B), indicating that submergence is only effective for shoot explants. To assess whether submergence induces wound responses, we analyzed the promoter activity of *JAZ10*, a widely used wound response marker gene (Mousavi et al., 2013). β-Glucuronidase (GUS) staining of *pJAZ10:GUS* transgenic seedlings after submergence showed similar GUS signals in control and submerged seedlings (Supplemental Figure 1C), indicating that submergence does not lead to wound responses.

We harvested the wound-proximal and wound-distal parts of the explants separately to analyze the expression of genes involved in cell fate transition by qRT–PCR. Expression of *WOX11*, the marker gene for cellular pluripotency acquisition (Liu et al., 2014), was significantly elevated only in the proximal part when seedlings were grown without submergence (Figure 1C and Supplemental Figure 1D). However, we observed a significant increase in *WOX11* expression during CIM incubation in the distal part of explants after submergence of intact seedlings for 1 h (Figure 1C). To verify the changes in *WOX11* expression after submergence, we analyzed GUS staining in *pWOX11:GUS* transgenic seedlings (Liu et al., 2014). Consistent with the expression analysis above, we detected GUS signals not only at the wound site but also in distal regions when seedlings were submerged shortly before leaf detachment (Figure 1D). To support our results, we analyzed the expression of other genes involved in cell fate transition. The expression levels of *LBD16*, *LBD29*, *PLETHORA 5* (*PLT5*), and *PLT7*, which are involved in induction of pluripotency and callus formation (Fan et al., 2012; Ikeuchi et al., 2017), were elevated in the distal part of explants after submergence (Figure 1E). These results indicate that short-term submergence activates cells distal to the wound site and reprograms their fate during CIM incubation. To investigate whether the effects of submergence on callus formation can also be observed in other species, we submerged Chinese cabbage (*Brassica rapa*) seedlings before detaching cotyledon explants and incubating them on CIM. Similar to *Arabidopsis*, we observed callus formation in regions distal to the wound site after submergence (Figure 1F), demonstrating that the effects of submergence on callus formation are not restricted to *Arabidopsis*.

Two different pathways can induce callus formation in explants. Auxin-induced callus formation occurs mainly in pericycle and pericycle-like cells through auxin-related lateral root developmental pathways, whereas wound-induced callus formation takes

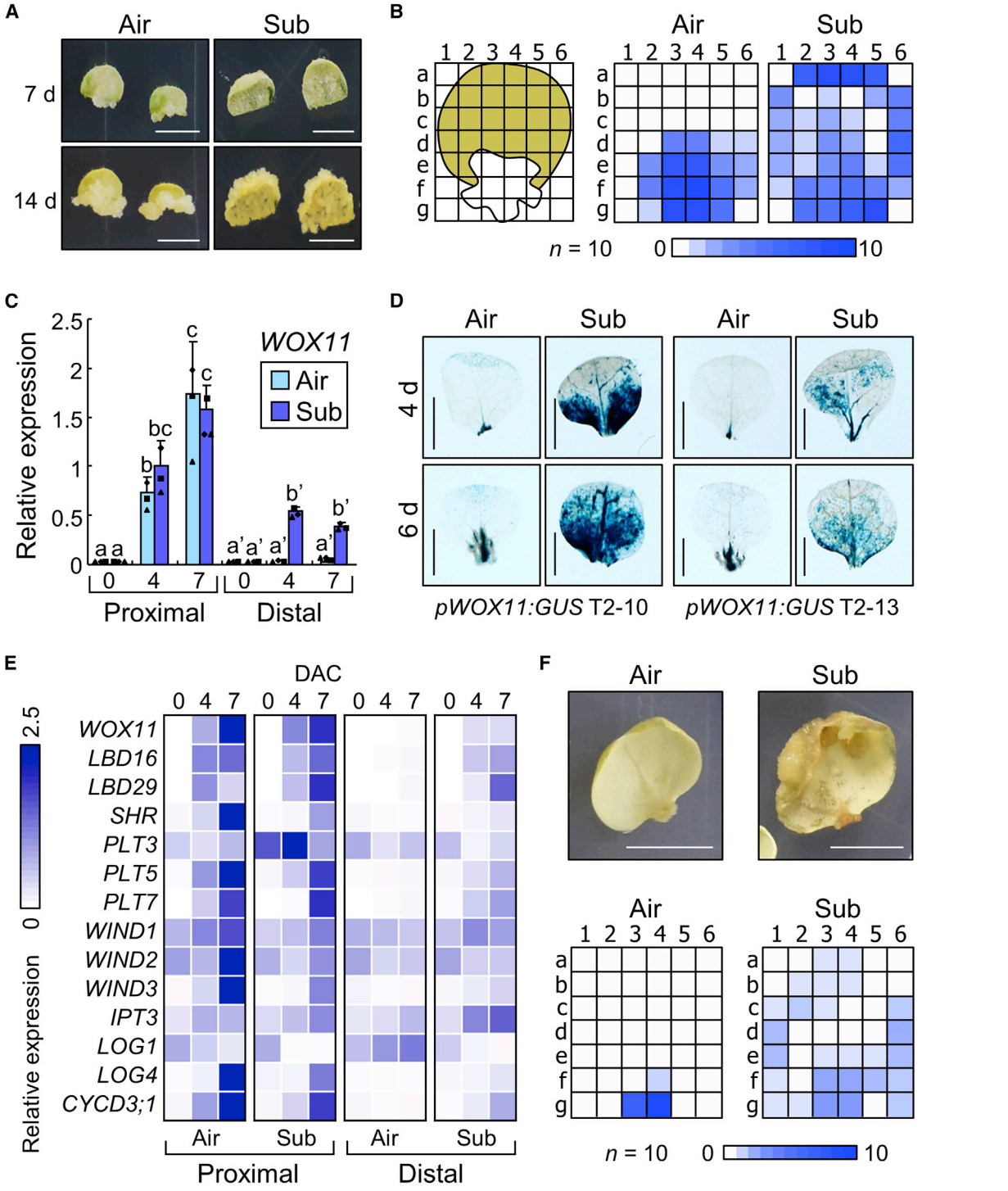

Figure 1. Submergence promotes callus formation in leaf explants.

(A–E) Wild-type Col-0 seedlings were submerged (Sub) or left in air (Air) for 1 h before leaf explants were incubated on callus-inducing medium (CIM).

(A) Representative images of explants. Scale bars, 0.5 cm.

(B and F) Callus formation in explants from submerged seedlings. The number of explants showing callus formation on each part of the explant 14 days after CIM incubation (DAC) is represented as a heatmap (n = 10).

(C) The distal and proximal parts of the explants were harvested separately to analyze *WOX11* expression (means + SD, n = 3 biological replicates, Tukey's test). The x axis indicates DAC.

(D) GUS staining of leaf explants from *pWOX11:GUS* seedlings. Scale bars, 0.2 cm.

(E) Average values of relative expression using two biological replicates, displayed as a heatmap.

(F) Callus formation on Chinese cabbage explants. Scale bars, 1 cm.

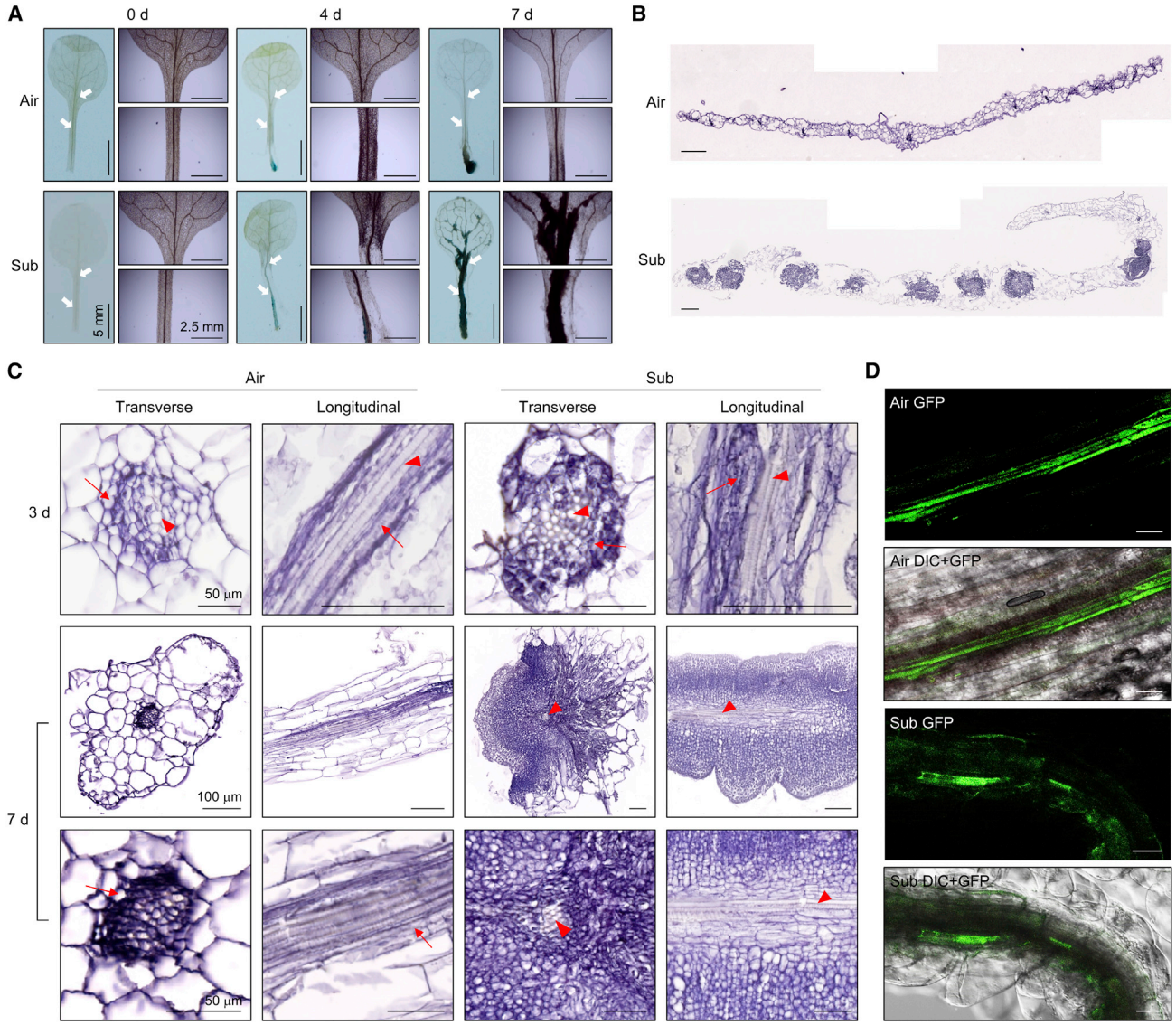

Figure 2. Submergence promotes callus formation in xylem pericycle cells.

Seedlings were submerged or left in air for 1 h, and then explants were incubated on CIM for the indicated times.

(A) GUS signals in *pCYCB1;1:GUS* seedlings at 0, 4, and 7 DAC. Arrows indicate regions magnified in the panels on the right.

(B) Transverse sections of the leaf blade at 7 DAC. Scale bars, 100 μm.

(C) Transverse and longitudinal sections of petioles at 3 and 7 DAC. Sections were stained with H&E. Magnified regions are also shown for sections at 7 DAC. Arrows indicate xylem pericycle; arrowheads indicate protoxylem.

(D) Confocal imaging of GFP signals in petioles from J0121 seedlings at 3 DAC. The part distal to the wound site was imaged. DIC, differential interference contrast. Scale bars, 50 μm.

place in multiple cell types through cytokinin signaling pathways (Atta et al., 2009; Sugimoto et al., 2010; Iwase et al., 2011). To investigate which pathway is related to submergence-promoted callus formation, we first analyzed promoter activity of the cell cycle marker gene *CYCLIN B1;1* (*CYCB1;1*) using *pCYCB1;1:GUS* transgenic seedlings (Ferreira et al., 1994; Kim et al., 2021). Although we observed the GUS signal only close to the wound site in control explants, we readily detected GUS staining in the vasculature of non-wounded regions after submergence (Figure 2A). This result indicates that submergence-promoted callus formation primarily occurs in the vasculature. To determine the cellular origin of the callus, we analyzed sections from *Arabidopsis* explants after CIM incubation. Consistent with the GUS assays, transverse sections showed that callus formation occurs in the vasculature of non-wounded regions after submergence (Figure 2B). Because the vasculature was too small to determine cell types, we used petiole explants in the following experiments. In non-wounded regions, callus cells started to form exclusively in xylem pericycle cells after submergence, whereas the protoxylem structure was not altered 3 days after CIM incubation (DAC; Figure 2C). At 7 DAC, exfoliation of tissues external to the pericycle and enlarged callus was observed after submergence. Confocal imaging of line J0121, a marker line in which the green fluorescent protein (GFP) gene is expressed in xylem-pole pericycle cells (Laplaze

et al., 2005), showed that the GFP signal in J0121 becomes diffuse, and its intensity decreases after submergence (Figure 2D). These results suggest that submergence promotes auxin-induced callus formation in xylem pericycle cells.

Submergence changes auxin responses

We next examined auxin signaling pathways in explants. We suspected that submergence might affect auxin transport during CIM incubation. However, treatment with *N*-1-naphthylphthalamic acid (NPA), an auxin transport inhibitor (Geldner et al., 2001), did not affect callus formation patterns regardless of submergence (Supplemental Figure 2A and 2B). Next we hypothesized that auxin perception might be affected by submergence. We determined that submergence raises expression of the auxin receptor genes *TRANSPORT INHIBITOR RESPONSE 1* (*TIR1*) and *AUXIN SIGNALING F-BOX 2* (*AFB2*) in the distal part of explants but slightly decreases their expression levels in the proximal part (Figure 3A). Because regulation of auxin receptor levels is critical for activating auxin signaling (Parry et al., 2009; Wang et al., 2016), we next examined auxin responses using explants from seedlings harboring the auxin output reporter $DR5_{rev}$:*GFP*. Consistent with the expression data, we observed activation of auxin signaling output in the distal part of the explants after the intact seedlings were submerged (Figure 3B and 3C). In contrast, auxin responses were largely restricted to the wound site when whole seedlings were maintained in air. These results suggest that submergence before leaf detachment activates auxin signaling in explants during CIM incubation, particularly in the part distal to the wound site.

To investigate whether the function of auxin receptors affects callus formation, we used the *tir1-1* mutant (Ruegger et al., 1998). Submergence induced callus formation in the distal part of wild-type explants, but the degree of callus formation decreased in *tir1-1* explants (Figure 3D). In contrast, we still observed callus formation in the wound-proximal part regardless of submergence status in *tir1-1* explants, suggesting that TIR1-mediated auxin signaling plays a key role in submergence-induced cell dedifferentiation in non-wounded sites during CIM incubation.

Ethylene controls callus formation

To identify the factors involved in submergence-promoted callus formation, we performed a transcriptome deep sequencing (RNA sequencing [RNA-seq]) analysis using intact wild-type seedlings after short-term submergence (Supplemental Table 1). Gene Ontology (GO) analysis of differentially expressed genes showed that the expression of genes involved in ethylene biosynthesis and response is highly induced by submergence (Supplemental Figure 3A and 3B), which is consistent with previous studies showing that submergence activates ethylene responses (Sasidharan and Voesenek, 2015; Lee et al., 2020).

Because short-term submergence before leaf detachment affected callus formation in leaf explants, we examined the expression of ethylene-related genes during CIM incubation. Expression of *1-AMINO-CYCLOPROPANE-1-CARBOXYLATE SYNTHASE 2* (*ACS2*), *ACS7*, and *ACS8*, which encode key enzymes involved in ethylene biosynthesis (Argueso et al., 2007), was significantly elevated in the distal part of explants from submerged seedlings. Expression of *ACS2* and *ACS7* increased in the distal and proximal parts of submerged seedlings (Supplemental Figure 3C). These results suggest that short-term submergence before leaf detachment induces ethylene biosynthesis in leaf explants during CIM incubation.

We then asked whether ethylene is involved in callus formation. To this end, we blocked ethylene signaling by adding $AgNO_3$, an ethylene perception inhibitor (Beyer, 1976). Submergence-induced callus formation in the distal part of explants diminished upon $AgNO_3$ treatment (Figure 4A). ACC supplementation increased the percentage of explants forming calli across the entire explant (Supplemental Figure 4A). The *ethylene-overproducer 1-1* (*eto1-1*) mutant also displayed callus formation similar to wild-type plants treated with ACC (Guzmán and Ecker, 1990; Supplemental Figure 4B). We next analyzed the phenotype of the ethylene receptor mutant *ethylene response 1-1* (*etr1-1*) (Rodríguez et al., 1999). We determined that the *etr1-1* mutant is insensitive to submergence, forming calli only near the wound site regardless of treatment (Supplemental Figure 4C). The expression of *WOX11* and auxin receptor genes at the distal part of explants was significantly reduced in *etr1-1* seedlings after submergence (Supplemental Figure 4D), suggesting that ethylene signaling is involved in regulation of auxin signaling. The *ctr1-1* mutation, which triggers a constitutive ethylene response (Kieber et al., 1993), induced pervasive callus formation in explants without submergence (Figure 4B). Consistent with this phenotype, the expression of *WOX11*, *TIR1*, and *AFB1* rose significantly in the distal part of *ctr1-1* explants at 7 DAC (Figure 4C). We observed induction of callus formation in non-submerged *ctr1-1* and submerged wild-type seedlings when the entire aerial part of the seedlings was incubated on CIM. Non-submerged wild-type seedlings, however, did not form calli except at wound sites (Figure 4D). These results suggest that ethylene activates auxin-mediated callus formation.

To verify the role of ethylene in callus formation, we used the ethylene-insensitive mutant *ein2-1* (Guzmán and Ecker, 1990). We submerged wild-type and *ein2-1* seedlings before incubating their leaf explants on CIM. The effects of submergence on callus formation in the distal part of explants were largely suppressed in *ein2-1* mutants (Figure 5A). Consistent with the callus formation patterns, the expression of *TIR1* and *AFB2* was higher in the distal part of the wild-type explants after submergence at 7 DAC but did not increase in *ein2-1* mutant explants (Figure 5B). Next we analyzed auxin responses in the *ein2-1* mutant explants using the $DR5_{rev}$:GFP reporter. Although submergence activates CIM-induced auxin responses across the entirety of wild-type explants, auxin responses in the distal part were largely suppressed in the *ein2-1* background (Figure 5C and 5D). These results suggest that submergence-induced activation of auxin signaling is dependent on EIN2 in non-wounded regions.

Post-transcriptional regulation of auxin receptors by ethylene

In the ethylene signaling pathway, EIN2 stabilizes the transcription factors EIN3 and EIL1 to regulate gene expression (Li et al., 2015; Merchante et al., 2015). Because the transcript levels of *TIR1* and *AFB2* are regulated by EIN2, we hypothesized that

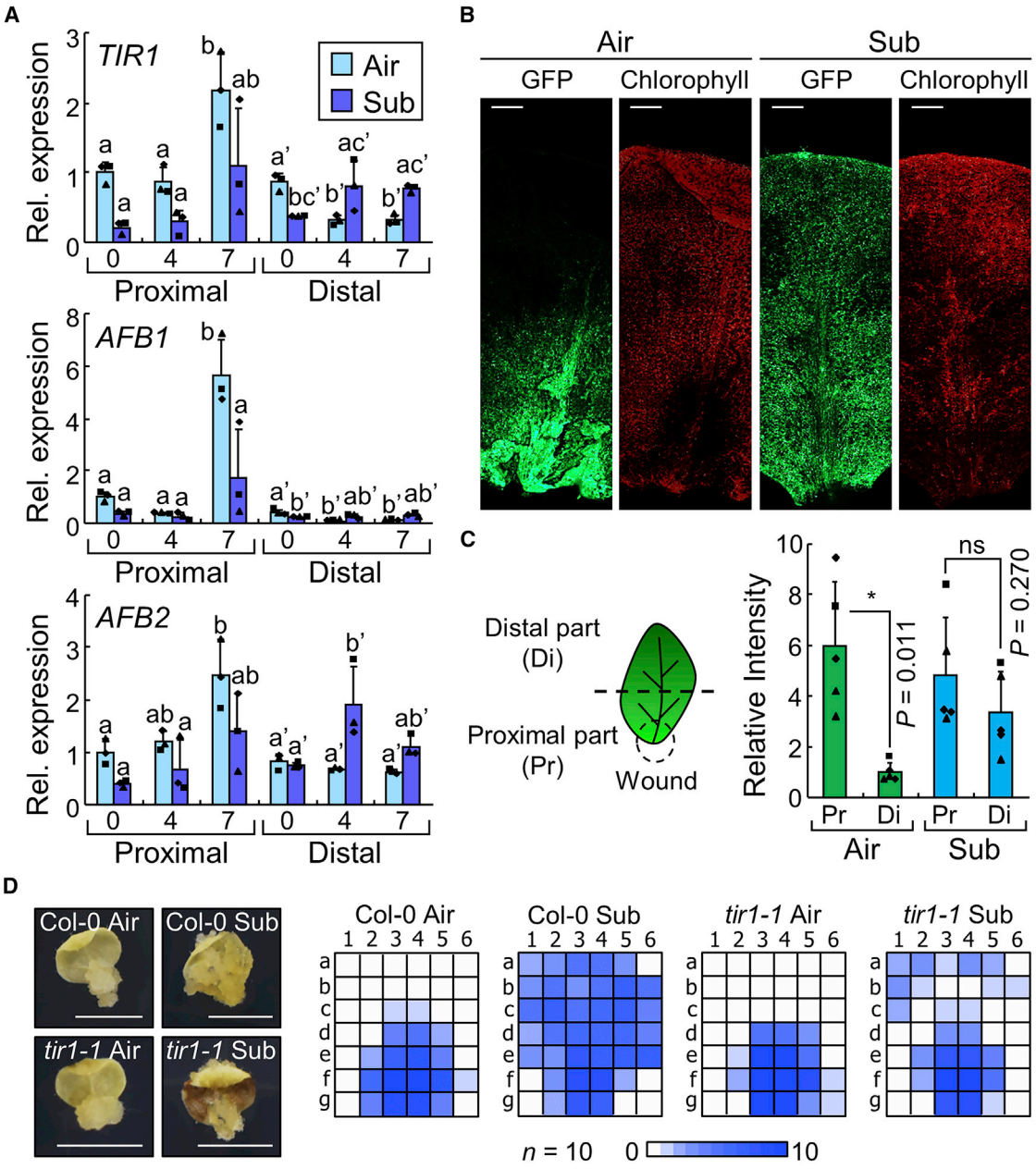

Figure 3. Submergence activates auxin responses during CIM incubation.

(A–D) Wild-type **(A and D)**, *DR5*$_{rev}$*:GFP* **(B and C)**, and *tir1-1* **(D)** seedlings were submerged or left in air for 1 h before leaf explants were incubated on CIM. **(A)** The distal and proximal parts of the explants were harvested at the indicated DAC for gene expression analysis (means + SD, $n = 3$ biological replicates, Tukey's test). **(B and C)** GFP and chlorophyll fluorescence analyzed at 4 DAC. **(B)** Montages of images. Scale bars, 0.3 mm. Orthogonal projections were generated from z stacks containing five images at intervals of about 16 μm. **(C)** Relative fluorescence intensity of GFP in the distal and proximal parts of the explants (means + SD, $n = 5$ biological replicates, Student's *t*-test). **(D)** Leaf explants were incubated on CIM for 12 days. Scale bars, 0.5 cm. The number of explants showing callus formation on each part is represented as a heatmap ($n = 10$).

EIN3 and EIL1 are also involved in these responses. However, the callus formation patterns of the *ein3 eil1* double mutant were similar to those of wild-type seedlings regardless of submergence (Supplemental Figure 5), suggesting that EIN3 and EIL1 are not related to submergence-mediated callus formation.

TIR1 and *AFB2* transcript levels are post-transcriptionally regulated by microRNA393 (miR393; Navarro et al., 2006; Parry et al., 2009). To examine whether submergence affects post-transcriptional regulation of these genes, we analyzed GUS signals in explants from *pTIR1:GUS tir1-1*, *pTIR1:TIR1-GUS tir1-1*, *pAFB1:GUS*, *pAFB1:AFB1-GUS*, *pAFB2:GUS*, and *pAFB2:AFB2-GUS* transgenic seedlings. In *pTIR1:GUS tir1-1* and *pAFB2:GUS* explants, we detected a broad GUS signal with localized high-intensity signals near the wound site, regardless of submergence (Figure 5E and Supplemental Figure 6). However, we only observed localized GUS signals near the wound site in *pTIR1:TIR1-GUS tir1-1* and *pAFB2:AFB2-GUS* explants under

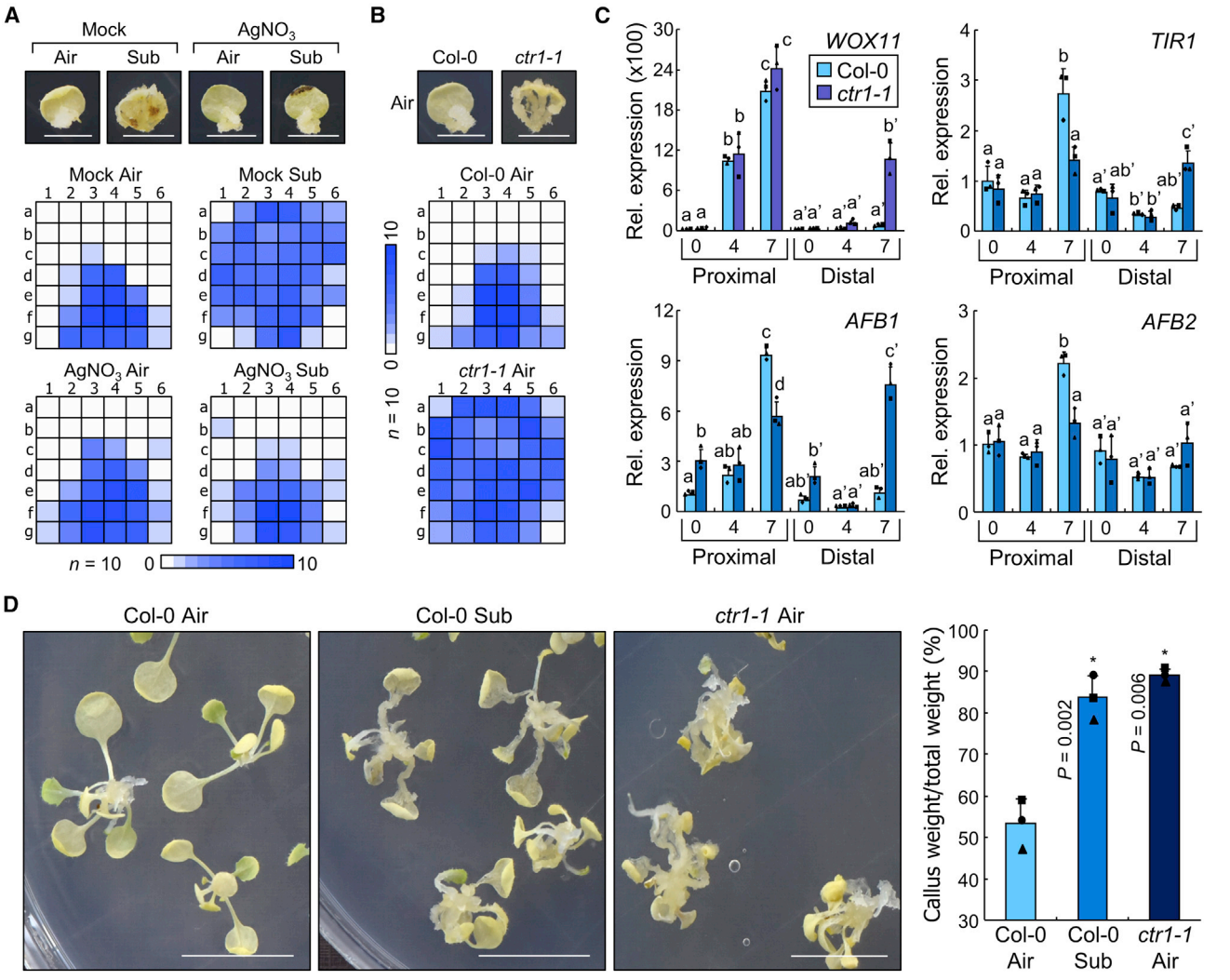

Figure 4. Ethylene promotes callus formation.

(A and B) the number of explants showing callus formation on each part is represented as a heatmap ($n = 10$). **(A)** Wild-type seedlings grown on MS-agar plates containing 10 μM $AgNO_3$ were submerged or left in air for 1 h before leaf explants were incubated on CIM containing 10 μM $AgNO_3$ for 12 days. Scale bars, 0.5 cm. **(B)** Leaf explants from *ctr1-1* seedlings grown without submergence were incubated on CIM for 12 days. Scale bars, 0.5 cm.

(C) Leaf explants from wild-type and *ctr1-1* seedlings grown without submergence were incubated on CIM. The distal and proximal parts of the explants were harvested at the indicated DAC for gene expression analysis (means + SD, $n = 3$ biological replicates, Tukey's test).

(D) Callus induction using whole shoots from seedlings. Wild-type seedlings were submerged or left in air for 1 h. The *ctr1-1* mutant seedlings were not submerged. Aerial parts of the seedlings were excised and placed on CIM in an inverted position. Photographs were taken at 12 DAC. Callus weight was divided by total plant weight (means + SD, $n = 3$ biological replicates, Student's *t*-test). Scale bars, 1 cm.

control conditions, although submergence induced spreading of GUS signals farther from the wound site. In contrast, *pAFB1:GUS* and *pAFB1:AFB1-GUS* explants exhibited broad GUS staining with and without submergence (Supplemental Figure 6). The *ein2-1* mutation suppressed GUS signals in the distal part of *pTIR1:TIR1-GUS* and *pAFB2:AFB2-GUS* explants after submergence but did not change the signal patterns in *pTIR1:-GUS* and *pAFB2:GUS* explants (Figure 5E and 5F). These results suggest that transcripts encoding the auxin receptors TIR1 and AFB2 are post-transcriptionally regulated by EIN2.

Because miR393 is a known repressor of auxin receptors, we analyzed the abundance of mature miR393 using the stem-loop qRT–PCR method (Varkonyi-Gasic et al., 2007). In wild-type explants, miR393 levels were higher in the distal part under control conditions compared with submergence (Figure 6A). Submergence significantly decreased miR393 levels in the distal part at 7 DAC (Figure 6A), which was consistent with observations of auxin receptor transcript levels (Figure 3A). The high levels of miR393 in the distal part were not affected by submergence in the *ein2-1* mutant (Figure 6B), indicating that EIN2 is an upstream regulator of miR393. Next we examined the role of miR393 in callus formation by overexpressing the mimicry construct *MIM393*, which mimics the target sites of miR393 and disturbs its function (Franco-Zorrilla et al., 2007; Wang et al., 2018). Incubation of *35S:MIM393* explants on CIM without submergence induced broader callus formation than in wild-type explants, spreading to the distal part (Figure 6C and

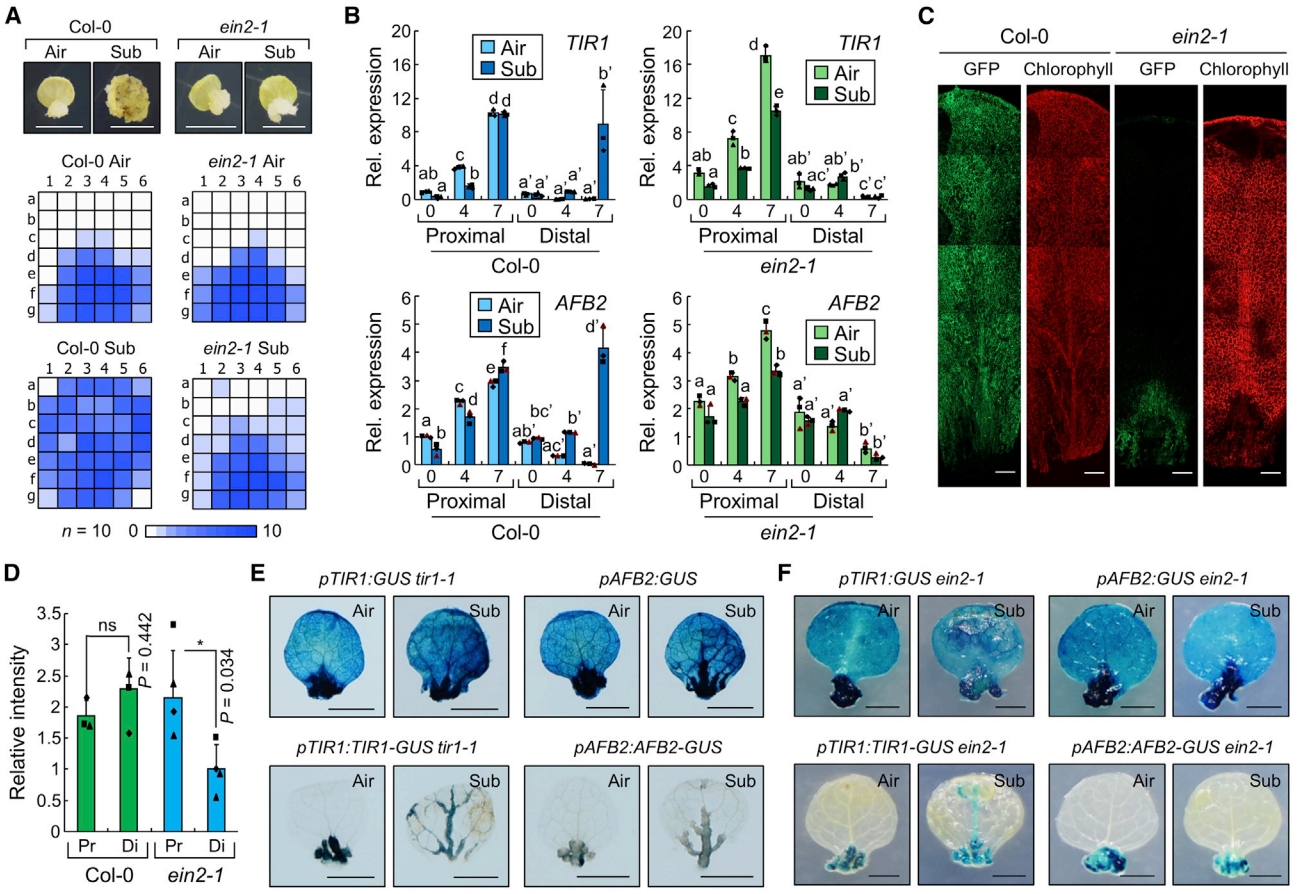

Figure 5. EIN2 post-transcriptionally regulates auxin receptors.

(A, B, E, and F) Seedlings were submerged or left in air for 1 h before leaf explants were incubated on CIM.

(A) Leaf explants from wild-type and *ein2-1* seedlings were incubated on CIM for 12 days. The number of explants showing callus formation on each part is represented as a heatmap (n = 10). Scale bars, 0.5 cm.

(B) The distal and proximal parts of the wild-type and *ein2-1* explants were harvested at the indicated DAC for gene expression analysis (means + SD, n = 3 biological replicates, Tukey's test).

(C and D) $DR5_{rev}$*:GFP* seedlings in the wild-type or *ein2-1* backgrounds were submerged for 1 h before leaf explants were incubated on CIM. The intensity of GFP and chlorophyll fluorescence was analyzed at 4 DAC. Scale bars, 0.3 mm. **(C)** Montages of images are displayed. Orthogonal projections were generated from z stacks containing five images at intervals of about 16 μm. **(D)** GFP fluorescence intensities in the proximal (Pr) and distal (Di) halves of the explants were measured (means + SD, n = 3–4 biological replicates, Student's t-test). ns, not significant.

(E and F) Leaf explants of *GUS*-expressing transgenic seedlings were subjected to GUS staining at 7 DAC. Scale bars, 0.2 cm.

Supplemental Figure 7A). Consistent with the callus formation patterns, the expression of *WOX11* and auxin receptor genes was significantly higher in the distal part of *35S:MIM393* explants, but their expression levels were not different from the wild type in the proximal part (Figure 5D and Supplemental Figure 7B). We introduced the *pTIR1:GUS*, *pTIR1:TIR1-GUS*, *pAFB2:GUS*, and *pAFB2:AFB2-GUS* transgenes in the *35S:MIM393* background and determined that suppression of miR393 function increases GUS signals in non-wounded regions of *pTIR1:TIR1-GUS* and *pAFB2:AFB2-GUS* explants without submergence (Figure 6E), confirming the role of miR393 in post-transcriptional regulation of auxin receptor genes. To verify the role of the miR393-auxin receptor module in callus formation, we generated *MIM393*-overexpressing plants in the *tir1-1* background (Supplemental Figure 7C). *MIM393* overexpression did not induce callus formation in non-wounded regions of *tir1-1* explants (Supplemental Figure 7D), suggesting that TIR1 acts downstream of miR393.

To examine how EIN2 controls miR393 abundance, we analyzed the expression of primary miR393A and miR393B transcripts (*pri-miR393A* and *pri-miR393B*). However, the expression levels of those transcripts were not significantly altered in the distal part of *ein2-1* explants after submergence (Supplemental Figure 8), suggesting that transcriptional control of miR393 is not the main function of EIN2. We also performed small RNA sequencing to determine whether EIN2-mediated regulation of miR393 is target specific. By comparing microRNA (miRNA) levels in the distal part of wild-type and *ein2-1* explants at 7 DAC, we established that EIN2 controls the abundance of 29 miRNAs, including miR393 (Supplemental Table 2). Based on the sequencing results, we searched for genes involved in non-specific regulation of miRNA abundance. SMALL RNA DEGRADING NUCLEASE 1 (SDN1) is an exoribonuclease that degrades multiple mature miRNAs (Ramachandran and Chen, 2008). HEN1 SUPPRESSOR1 (HESO1) is a nucleotidyl transferase that uridylates unmethylated miRNAs for degradation

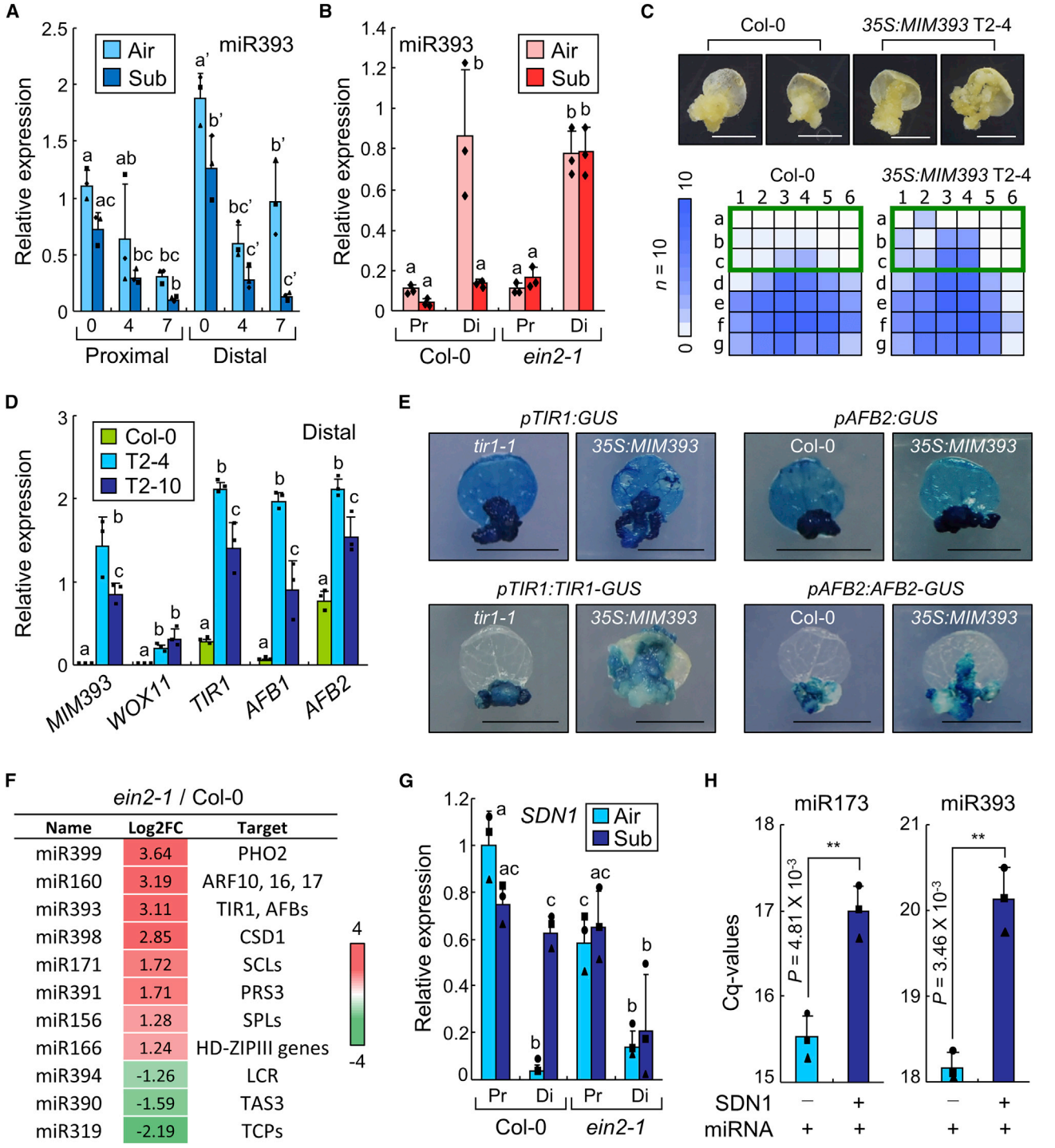

Figure 6. EIN2 controls miR393 abundance.

(A, B, and G) Seedlings were submerged or left in air for 1 h.

(C–E) Seedlings grown without submergence were used.

(A and B) Leaf explants from wild-type **(A and B)** and *ein2-1* **(B)** seedlings were incubated on CIM. The distal and proximal parts of the explants were harvested separately at the indicated DAC **(A)** or at 7 DAC **(B)** for analyzing miR393 abundance (means + SD, $n = 3$ biological replicates, Tukey's test).

(C and D) Leaf explants from wild-type and *35S:MIM393* seedlings were incubated on CIM for 17 days **(C)** or 7 days **(D)**. The number of explants showing callus formation on each part is represented as a heatmap **(C)**. Green squares indicate parts distal to the wound site. Scale bars, 0.5 cm. The distal and

(legend continued on next page)

(Zhao et al., 2012). Under our experimental conditions, expression of *SDN1* and *HES O 1* increased in the distal part of wild-type explants after submergence but remained low in *ein2-1* mutant explants (Figure 6G and Supplemental Figure 9), which was the opposite of miR393 levels (Figure 6B). *In vitro* ribonuclease activity assays showed that SDN1 directly degrades mature miR393 (Figure 6H). Consistent with these results, transcriptional overexpression of *MIR393A* did not suppress callus formation in non-wounded regions after submergence (Supplemental Figure 10A and 10B), suggesting that post-transcriptional control of miR393 is important in regulation of callus formation. These results suggest that EIN2 facilitates miR393 degradation in non-wounded regions of explants after submergence by regulating the expression of genes related to miRNA turnover, like *SDN1*.

Regeneration capacity of submergence-induced calli

The regeneration capacity of calli is a bottleneck for *de novo* shoot organogenesis and generation of transgenic plants in most crop species (Radhakrishnan et al., 2018; Shin et al., 2020). Because callus formation occurs rapidly near wound sites, the distal/non-wounded part of explants cannot be used effectively for *de novo* shoot organogenesis, which is important for biotechnological approaches to crop improvement (Shin et al., 2020). Based on our data showing that submergence induces callus formation across the entirety of explants, we investigated whether submergence-induced calli are competent for shoot regeneration. Accordingly, we incubated leaf explants from wild-type seedlings treated with short-term submergence on CIM, transferred to shoot-inducing medium, and incubated them until we observed shoot regeneration. *De novo* shoot organogenesis occurred in calli from the distal and proximal parts of the explants in submergence-treated groups, whereas callus formation and shoot regeneration occurred only in the proximal part of control explants (Figure 7A–7C). These results indicate that submergence-induced calli can be used for *de novo* shoot organogenesis.

DISCUSSION

Our study revealed that short-term submergence and ethylene promote callus formation in shoot explants. Short-term submergence of intact seedlings induced ethylene biosynthesis and concomitant activation of ethylene signaling in the explants, which facilitated miR393 degradation during CIM incubation (Figure 7D). These processes led to accumulation of auxin receptor transcripts, which promoted auxin-mediated callus formation across the entire explant. We propose a new approach to boosting callus formation efficiency in shoot explants, which can be applied to shoot regeneration and generating transgenic plants.

Our results showed that EIN2 played a critical role in ethylene-mediated callus formation; but EIN3 and EIL1 were not involved in these processes. Previous reports have shown that EIN2 and EIN3/EIL1 have different functions. For instance, etiolated *Arabidopsis* hypocotyls exhibit two phases of ethylene-mediated growth inhibition, but EIN3 and EIL1 only participate in the second phase, whereas EIN2 regulates both phases (Binder et al., 2004). EIN2 upregulates expression of genes encoding NAC (NAM, ATAF1, -2, and CUC2) domain-containing proteins (NACs), including NAC019, NAC047, and NAC055, during leaf senescence, but their expression is independent of EIN3 (Kim et al., 2014). In this study, expression of *SDN1* was upregulated by EIN2 after submergence (Figure 6G), which might be the reason for the observed decrease in miR393 levels (Figure 6B). Because EIN2 directly binds to *EIN3-BINDING F BOX PROTEIN 2* transcripts outside of the nucleus (Merchante et al., 2015), it is possible that EIN2 also controls the stability of *SDN1* mRNA in the cytosol. Investigation of EIN2-interacting RNAs during CIM incubation will be necessary to fully identify the molecular mechanisms of EIN2-dependent callus formation after submergence.

Our data showed that miR393 controlled callus formation, but the effects of miR393 inhibition were not as strong as those of ethylene signaling activation (Figure 4B and 6C). This observation suggested that additional factors are involved in these responses. In this study, small RNA-seq showed that 29 miRNAs were differentially abundant in the *ein2-1* mutant. Among them, miR160 is a negative regulator of the *AUXIN RESPONSE FACTOR* family of transcription factor genes, whose encoded proteins activate auxin signaling and callus formation (Wang et al., 2005; Liu et al., 2016). Therefore, miR160 may also participate in ethylene-mediated control of cell dedifferentiation, which possibly explains the weak phenotype observed after suppression of miR393 function. EIN2 upregulated the expression of *SDN1* and *HES O 1* (Figure 6G and Supplemental Figure 9), which are related to degradation of multiple miRNAs (Ramachandran and Chen, 2008; Zhao et al., 2012). Considering previous reports and the data presented here, we propose that EIN2 acts as a central regulator of ethylene signaling that controls complex molecular events related to miRNA turnover to induce callus formation in non-wounded regions. A deeper understanding of EIN2 function, however, will be required to identify its direct targets.

Although we defined a regulatory pathway for callus induction in non-wounded regions, the molecular mechanisms underlying

proximal parts of the explants were harvested separately for gene expression analysis (**D**; means + SD, $n = 3$ biological replicates, Tukey's test). See Supplemental Figure 7B for expression in the proximal parts.

(E) Leaf explants from *GUS*-expressing seedlings were subjected to GUS staining at 12–14 DAC. Scale bars, 0.5 cm.

(F) Wild-type and *ein2-1* seedlings were submerged for 1 h before leaf explants were incubated on CIM. The distal part of explants was harvested at 7 DAC. Representative miRNAs that showed differential abundance in *ein2-1* are listed. Average Log2 fold change is displayed as a heatmap ($n = 3$). Scale bar, Log2 fold change.

(G) Leaf explants from wild-type and *ein2-1* seedlings were incubated on CIM. The distal and proximal parts of the explants were harvested at 7 DAC for gene expression analysis (means + SD, $n = 3$ biological replicates, Tukey's test).

(H) *In vitro* ribonuclease activity assay, performed using purified recombinant MBP-His-SDN1 and mature miR393. miR173 was used as a positive control. After the reaction, the amount of mature miRNA was measured using the stem-loop qRT–PCR method (means + SD, $n = 3$ technical replicates, Student's *t*-test).

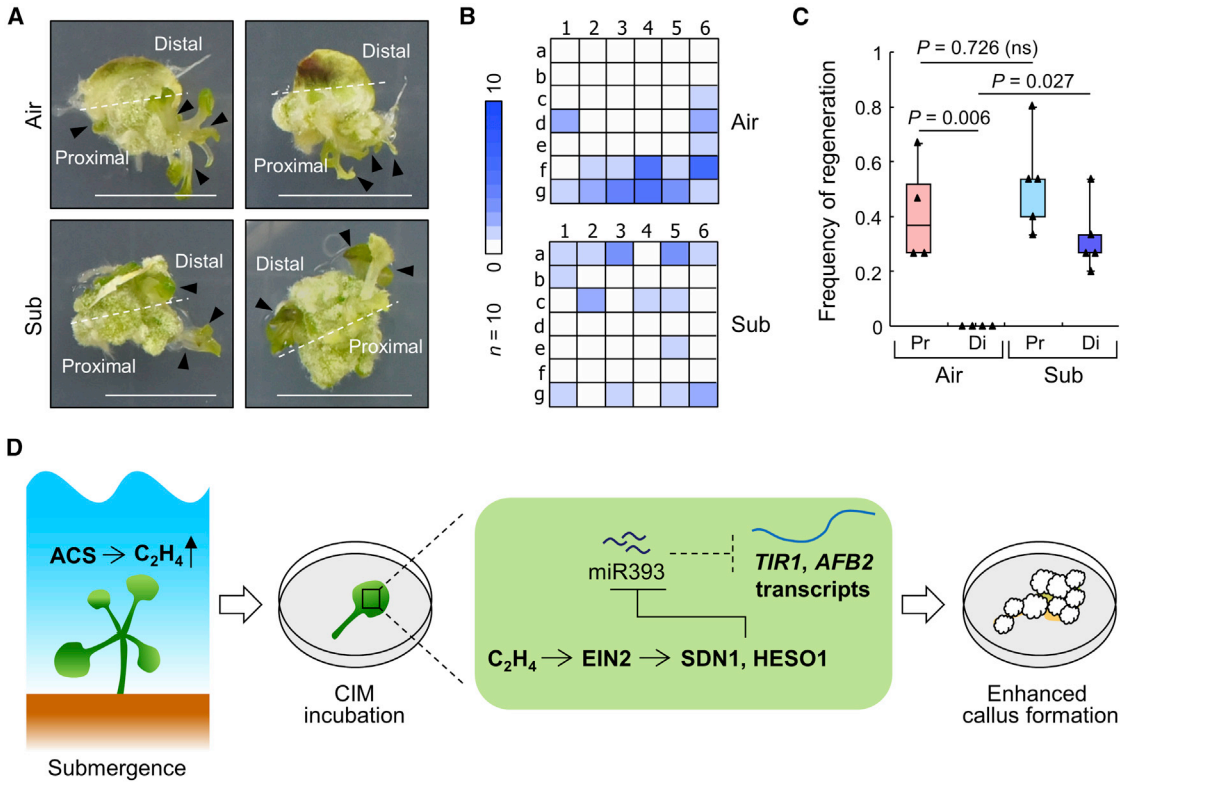

Figure 7. Shoot regeneration from the submergence-induced callus.

(A) Representative images of shoot regeneration of explants from submerged seedlings. Scale bars, 1 cm.

(B) Shoot regeneration patterns in explants from submerged seedlings. The number of explants showing shoot emergence on each part is represented by a heatmap (n = 10).

(C) Frequency of regeneration, calculated as the number of explants that regenerated at least one shoot from the distal or proximal part divided by the total number of explants (means + SD, n = 4–5 biological replicates, Tukey's test). Approximately 15 explants were used for each biological replicate.

(D) A proposed model illustrating the possible mechanisms underlying submergence-promoted callus formation. Submergence induces expression of *ACS* genes to produce ethylene. During CIM incubation after submergence, activated ethylene signals facilitate miR393 degradation through induction of genes related to miRNA turnover. These processes lead to accumulation of *TIR1* and *AFB2* transcripts, which promotes auxin-induced callus formation.

callus formation at wound sites under normal conditions are still unclear. Based on our expression analyses, low miR393 levels and high auxin receptor transcript levels at the wound site would be expected to promote callus formation (Figures 3A, 5E, and 6A). However, expression of these genes was not particularly affected by the *ein2-1* mutation (Figures 5B, 5E, and 6B), suggesting that there are additional mechanisms to locally induce callus formation at wounded regions. The *tir1-1* mutation caused only minor effects on callus formation under normal conditions (Figure 3D), suggesting that the unknown wound-related signals may also control downstream targets of auxin signaling. A possible candidate is JA, which is rapidly synthesized after wounding and activates defense responses against herbivores (Mithöfer and Boland, 2012). JA promotes auxin production through upregulation of *ETHYLENE RESPONSE FACTOR 109* expression, particularly at the wound site, to induce root organogenesis (Zhang et al., 2019). Mutation of the JA receptor *CORONATINE INSENSITIVE 1* leads to defects in callus formation in leaf explants (Hernández-Coronado et al., 2022), supporting a relationship between JA and callus formation. Therefore, combinatorial effects of JA and ethylene at the wounded and non-wounded regions, respectively, may be key factors in spatial regulation of callus formation in shoot explants, although more evidence is needed to support this hypothesis.

METHODS

Plant materials

Col-0 was used as a wild type *Arabidopsis* plant. *tir1-1* (Ruegger et al., 1998; N3798), *pTIR1:GUS tir1-1* (Parry et al., 2009; N69675), *pTIR1:TIR1-GUS tir1-1* (Parry et al., 2009; N69679), *pAFB1:GUS* (Parry et al., 2009; N69676), *pAFB1:AFB1-GUS* (Parry et al., 2009; N69680), *pAFB2:GUS* (Parry et al., 2009; N69677), *pAFB2:AFB2-GUS* (Parry et al., 2009; N69681), and *etr1-1* (N237) were obtained from the Nottingham Arabidopsis Stock Centre. $DR5_{rev}$:GFP (Friml et al., 2003; CS9361) and *eto1-1* (CS3072) were obtained from the Arabidopsis Biological Resource Center. *ctr1-1* (Kieber et al., 1993), *ein2-1* (Guzmán and Ecker, 1990), and *ein3-1 eil1-3* (Jeong et al., 2010) were a gift from Dr. Young-Joon Park. *pCYCB1;1:GUS* was a gift from Dr. Mi-Jeong Jeong (Kim et al., 2021). The *pWOX11:GUS*, *35S:MIM393*, and *35S:MIR393A* transgenic plants were generated by *Agrobacterium*-mediated transformation of the corresponding vectors.

Plasmid construction

To generate the *35S:MIM393* construct, the artificial miRNA target mimic strategy was used (Franco-Zorrilla et al., 2007). Primers were designed to mimic mature miR393 target-binding sequences. First PCR products were

generated using IPS1-F (5′-CACCAAGAAAAATGGCCATCCCCTAGC-3′) and MIM393-I (5′-CTTCCAAAGGGAGGGCCGCATTGATCCTTTCTA-GAGGGAGATAA-3′) primers, and second PCR products were generated using MIM393-II (5′- AAGGATCAATGCGGCCCTCCCTTTGGAAGCTTCG GTTCCCCTCG-3′) and IPS1-R (5′- GAGGAATTCACTATAAAGAG AATCG-3′) primers. First and second PCR products were combined, and PCR was performed using IPS1-F and IPS1-R primers to generate the *MIM393* construct. The *MIM393* construct was cloned into pENTR/SD/D-Topo. The *MIM393* fragment was amplified and cloned into the myc-pBA vector (Jung et al., 2013) using XhoI and AvrII restriction enzymes. To generate the *pWOX11:GUS* construct, approximately 4.87-kb sequences upstream of the translational start site of the *WOX11* gene were amplified using pWOX11-F (5′-AATGGATCCCTAACTGTTAC-GATTGAATTCAAACGATA-3′) and pWOX11-R (5′-TTGGCGCGCCTG CTTTGAAGAATATTGATATTATCTGGTG-3′). The PCR products were fused to the 5′ ends of the *GUS* gene using BamHI and AscI restriction enzymes in the pBA002a-GUS vector. To generate the *35S:MIR393A* construct, the coding sequence of the *MIR393A* gene was amplified using pMIR393A-F (5′-AATTCTCGAG CTACGTACCCATCATGAACACTGT-3′) and pMIR393A-R (5′-AATTCCTAGG ACTTCTTCTTCTTTTTTGGTTT TGC-3′), and the PCR products were cloned into the myc-pBA vector using XhoI and AvrII restriction enzymes.

Agrobacterium-mediated transformation of *Arabidopsis*

The *35S:MIM393*, *pWOX11:GUS*, and *35S:MIR393A* vector constructs were transferred to *Agrobacterium* strain GV3101. The floral dip method (Zhang et al., 2006) was used to transfer the vector constructs. Transgenic plants were selected using phosphinothricin (P-165-250, Gold Biotechnology). Three independent transgenic plants were obtained, and two independent lines were analyzed.

Plant growth conditions

Arabidopsis plants were grown on half-strength MS (Murashige and Skoog)-agar medium containing 0.7% plant agar. Seeds were pre-incubated at 4°C for 3 days for stratification. After cold incubation, plants were grown under long-day conditions (16 h light, 8 h dark) at 24°C with ~100 μmol m^{-2} s^{-1} light intensity in the growth room. Plants were grown for 2 weeks, and the first pair of leaves was used for leaf explants. The petiole-blade junction was excised to produce leaf explants. For Chinese cabbage, the Jangsaeng-3-ho cultivar (Lee and Hong, 2015; Asia Seed) was grown under conditions identical to those used for *Arabidopsis* for 9 days. Cotyledons were used as explants.

Incubation of leaf explants for callus formation

To induce callus formation, *Arabidopsis* explants were incubated on CIM (B5 medium, 3% sucrose, 0.05 mg l^{-1} kinetin, 0.5 mg l^{-1} 2,4-dichlorophenoxyacetic acid, 0.7% agar, and pH 5.8 using KOH) with the adaxial side in contact with the medium under darkness for 12 days in most of the assays. When the explants were incubated for different time periods, details are described in the figure legend. For analysis of gene expressions during callus formation, the distal (distant from the wound site) and proximal (containing the wound site) parts of the explants were harvested separately at the indicated time points as indicated in the figures. For callus induction of Chinese cabbage, cotyledons were incubated on CIM for 14 days. For *de novo* shoot organogenesis, *Arabidopsis* Col-0 explants were incubated on CIM with the adaxial side in contact with the medium for 7 days in darkness. After CIM incubation, explants were transferred to shoot-inducing medium (B5 medium, 2% glucose, 0.9 mmol l^{-1} indole-3-acetic acid, 2.5 mmol l^{-1} 2-isopentenyladenine, 0.4% agar, and pH 5.8 using KOH) and further incubated for 14 days under long-day conditions with ~100 μmol m^{-2} s^{-1} light intensity. For submergence, *Arabidopsis* and Chinese cabbage plants grown on MS-agar plates were submerged by pouring distilled water into the plates, and then they were incubated for 1 h. After submergence, water was removed, and leaves (for *Arabidopsis*) or cotyledons (for Chinese cabbage) were excised to generate explants. For incubation of aerial part of the seedlings, aerial parts of the 2-week-old seedlings were excised and placed on CIM with the adaxial side in contact with the medium. Explants were incubated for 12 days in darkness.

Pharmacological treatment

For ACC and $AgNO_3$ treatment, Col-0 seedlings were grown in MS-agar plates containing 10 μM ACC (A3903, Sigma-Aldrich) or $AgNO_3$ (S7276, Sigma-Aldrich) for 2 weeks. Seedlings were submerged or left in the air for 1 h, and then leaf explants were incubated on CIM containing 10 μM ACC or $AgNO_3$ for 12 days in darkness. For NPA treatment, Col-0 seedlings grown in MS-agar plates for 2 weeks were submerged or left in the air for 1 h. Leaf explants were incubated on CIM containing DMSO (mock) or 25 μM NPA (33 371, Sigma-Aldrich) for 12 days in darkness.

Visualizing callus formation patterns

Explants were photographed, and the images were divided into 6 × 7 sections as displayed in Figure 1B. Ten explants were used for the analysis. All explants were oriented similarly. Each section was analyzed for callus formation. Ten explants were analyzed, and the number of explants showing callus formation on each section was visualized as a heatmap. For visualizing shoot emergence patterns, each image section was analyzed for green shoot emergence. Ten explants were analyzed, and the number of explants showing shoot emergence on each section was visualized as a heatmap.

RNA extraction and gene expression analysis by quantitative PCR

Total RNA was extracted from the plant materials using Trizol (Thermo Fisher Scientific) according to the manufacturer's recommendations. First-strand complementary DNA synthesis was performed using AccuPower CycleScript RT PreMix (Bioneer) according to the manufacturer's protocol. Quantitative PCR (qPCR) was performed using TOPreal qPCR 2X PreMIX (SYBR Green with low 5-carboxy-x-rhodamine (ROX), Enzynomics). Primers used for qPCR are listed in Supplemental Table 3. Gene expression was normalized using *UBQ10* as a reference gene.

Thin sectioning and imaging

Explants were fixed with paraformaldehyde (PFA) fixative (4% PFA, 0.25% glutaraldehyde, 0.1% Triton-X 100, and 0.1% Tween 20) and then dehydrated in a graded ethanol series (30%, 50%, 70%, 85%, 95%, and 100%). Tissues were infiltrated and embedded with paraffin. The paraffin block containing tissues was sliced into 10-μm-thick sections using a microtome (RM2125RT, Leica). Sections were then deparaffinized in a graded ethanol series (100%, 95%, 90%, 80%, 60%, and 30%) and hydrated in distilled water. Tissues were stained using the H&E Staining Kit (ab245880; Abcam). Imaging of the stained sections was performed using a slide scanner (Axio Scan Z1, Carl Zeiss).

Stem-loop qRT–PCR

Stem-loop qRT–PCR was performed as described in a previous report (Varkonyi-Gasic et al., 2007) with modifications. Leaf explants were incubated on CIM for the time periods indicated in the figures. The distal and proximal parts of the explants were harvested separately. Total RNA was extracted from the explants using the miRNeasy Mini Kit (QIAGEN). The stem-loop RT primers specific for miR173 (5′-GTCGTATCCAGTGCAGGGTCCGAGGTATTCGCACTGGATACGACGTG ATT-3′) or miR393 (5′-GTCGTATCCAGTGCAGGGTCCGAGGTATTCG-CACTGGATACGACGGATCA-3′) were used for first-strand complementary DNA synthesis. The stem-loop RT primer was mixed with total RNA, and the mixture was heated at 65°C for 5 min and then incubated on ice for annealing of the primers to miRNAs. After annealing, complementary DNA synthesis was performed with SuperScript IV reverse transcriptase (Thermo Fisher Scientific). For negative control reactions, the annealed primer-RNA mixture was mixed with distilled water instead of the reverse transcriptase. For qPCR, a miRNA-specific forward primer and general reverse primer were used (Supplemental Table 3). Addition

of 6 bp of flanking sequences at the 5′ end of the forward primer is important for highly specific qPCR reactions. For normalization of miRNA expression, first-strand complementary DNA was synthesized using AccuPower CycleScript RT PreMix (Bioneer) according to the manufacturer's protocol with the same amount of total RNA as used for stem-loop RT reactions, and qPCR was performed using *UBQ10* primers (Supplemental Table 3). The expression of miR393 was normalized using *UBQ10* as a reference gene.

GUS staining

Plant materials were fixed in 90% acetone for 20 min on ice and then washed twice using rinsing solution containing 50 mM sodium phosphate (pH 7.2), 0.5 mM $K_3Fe(CN)_6$, and 0.5 mM $K_4Fe(CN)_6$. Washed plant tissues were completely submerged in staining solution containing 2 mM X-Gluc (Duchefa) in the rinsing solution and incubated at 37°C for 16 h. Plant materials were then incubated in 70% ethanol for 24 h to remove chlorophyll. Stained plant tissues were mounted on slide glasses and photographed using a Nikon D750 digital camera.

Fluorescence imaging

Explants were mounted on slide glasses with 50–100 μl of water and covered with cover glass. The abaxial sides of the leaf explants were observed. GFP and chlorophyll fluorescence imaging was performed using an LSM 800 confocal microscope (Carl Zeiss). The excitation and emission wavelengths were 488 and 500–600 nm, respectively. For analyzing chlorophyll fluorescence, the excitation and emission wavelengths were 561 and 560–700 nm, respectively. Fluorescence images were analyzed using the ZEN 2.5 LITE software. To measure the fluorescence intensity of GFP signals, ImageJ software was used.

RNA-seq

For sequencing mRNAs and small RNAs, total RNA was extracted using the RNeasy Plant Mini Kit (QIAGEN) and the miRNeasy Kit (QIAGEN), respectively. The RNA samples were subjected to RNA-seq by Seeders. Library construction was performed using 1 μg of total RNA using the Illumina mRNA Sample Prep Kit (Illumina). For small RNA-seq, the TruSeq Small RNA Library Prep Kit (Illumina) was used. Raw RNA-seq data were produced using the Illumina Hiseq X platform. Sequencing adapters and low-quality bases in the raw reads were trimmed. High-quality reads were mapped to the TAIR10 reference genome (https://www.arabidopsis.org). For small RNA-seq, only 15- to 30-nt reads were used for analysis. GO was analyzed using the Biological Networks Gene Ontology tool with Benjamini-Hochberg-corrected $p < 0.01$. Significantly overrepresented GO terms were displayed with the network diagram.

In vitro ribonuclease activity assay

The ribonuclease activity assay was performed as described previously (Ramachandran and Chen, 2008). The reaction mixture containing 50 mM Tris-HCl (pH 8.0(, 135 mM KCl, 2.5 mM $MgCl_2$, 2.5% glycerol, BSA (1 μg μl^{-1}), RNaseOUT (40 units, Invitrogen), synthesized mature miRNA substrates (0.05 pmol μl^{-1}), and recombinant MBP (maltose-binding protein)-His-SDN1 protein (3.33 ng μl^{-1}) was incubated at 37°C for 1 h. The miRNA was purified using the miRNeasy Kit (QIAGEN). The amount of miRNA was quantified using the stem-loop qRT–PCR method.

Statistical analysis

All statistical methods and the number of biological replicates in each assay are described in the figure legends. One-way ANOVA with post hoc Tukey's test was performed using Rstudio software. Letters in bar plots indicate groups that are statistically significantly different from each other ($p < 0.05$). Student's *t*-test was performed using Microsoft Excel (*$p < 0.05$). Bar plots and boxplots were made using Microsoft Excel. For boxplots, each box is bounded by the lower and upper quartiles, and the center line represents the median. Whiskers indicate minimum and maximum values. The heatmap was made using Java Treeview. Individual data points were included in all plots.

Data availability

All data generated during this study are included in this article and the Supplemental information. The raw and processed RNA-seq data have been deposited in NCBI's Gene Expression Omnibus and are accessible through GEO series accession number GSE182724. Small RNA-seq data were deposited in the GEO repository (GSE210413).

ACCESSION NUMBERS

The *Arabidopsis* Genome Initiative locus identifiers for the genes mentioned in this article are as follows: AT3G03660 (WOX11), AT2G42430 (LBD16), AT3G58190 (LBD29), AT4G37650 (SHR), AT5G10510 (PLT3), AT5G57390 (PLT5), AT5G65510 (PLT7), AT1G78080 (WIND1), AT1G22190 (WIND2), AT1G36060 (WIND3), AT3G63110 (IPT3), AT2G28305 (LOG1), AT3G53450 (LOG4), AT4G34160 (CYCD3; 1), AT3G62980 (TIR1), AT4G03190 (AFB1), AT3G26810 (AFB2), AT5G03730 (CTR1), AT5G03280 (EIN2), AT3G20770 (EIN3), AT2G27050 (EIL1), AT3G51770 (ETO1), AT1G66340 (ETR1), AT1G01480 (ACS2), AT4G26200 (ACS7), AT4G37770 (ACS8), AT2G39885 (MIR393A), AT3G55734 (MIR393B), AT3G50100 (SDN1), and AT2G39740 (HESO1).

SUPPLEMENTAL INFORMATION

Supplemental information is available at *Molecular Plant Online*.

FUNDING

This work was supported by the Basic Research Program provided by the National Research Foundation of Korea (NRF-2019R1C1C1002045 and NRF-2021R1A2C4002413), the New Breeding Technologies Development Program (project PJ0165302022) provided by the Rural Development Administration of Korea, and the KRIBB Research Initiative Program (KGM5372221).

AUTHOR CONTRIBUTIONS

S.Y.S. and H.-J.L. conceived the study and wrote the manuscript. S.Y.S. and H.-J.L. generated transgenic plants and analyzed callus formation phenotypes and performed gene expression analysis, GUS staining, and confocal microscopy. Y.C. and S.-G.K. performed imaging of explant sections. S.-J.P. and J.-S.P. carried out *de novo* shoot organogenesis assays. K.-B.M., H.-S.K., J.H.J., and H.S.C. provided experimental equipment and participated in scientific discussions.

ACKNOWLEDGMENTS

We thank Dr. Young-Joon Park for providing *ctr1-1*, *ein2-1*, and *ein3-1 eil1-3* seeds; Dr. Mi-Jeong Jeong for providing *pCYCB1;1:GUS* seeds; and Hyang Ran Yoon for managing confocal microscopy. We acknowledge the facilities and the scientific and technical assistance of the EM & Histology Core Facility and Dr. Yongsuk Hur at the BioMedical Research Center, KAIST. No conflict of interest is declared.

Received: September 30, 2022
Revised: November 1, 2022
Accepted: November 1, 2022
Published: November 4, 2022

REFERENCES

Adkins, S.W., Kunanuvatchaidach, R., Gray, S.J., and Adkins, A.L. (1993). Effect of ethylene and culture environment on rice callus proliferation. J. Exp. Bot. **44**:1829–1835.

Alonso, J.M., Hirayama, T., Roman, G., Nourizadeh, S., and Ecker, J.R. (1999). EIN2, a bifunctional transducer of ethylene and stress responses in *Arabidopsis*. Science **284**:2148–2152.

Argueso, C.T., Hansen, M., and Kieber, J.J. (2007). Regulation of ethylene biosynthesis. J. Plant Growth Regul. **26**:92–105.

Atta, R., Laurens, L., Boucheron-Dubuisson, E., Guivarc'h, A., Carnero, E., Giraudat-Pautot, V., Rech, P., and Chriqui, D. (2009). Pluripotency of *Arabidopsis* xylem pericycle underlies shoot

regeneration from root and hypocotyl explants grown *in vitro*. Plant J. **57**:626–644.

Beyer, E.M. (1976). A potent inhibitor of ethylene action in plants. Plant Physiol. **58**:268–271.

Binder, B.M., Mortimore, L.A., Stepanova, A.N., Ecker, J.R., and Bleecker, A.B. (2004). Short-term growth responses to ethylene in *Arabidopsis* seedlings are EIN3/EIL1 independent. Plant Physiol. **136**:2921–2927.

Binder, B.M. (2020). Ethylene signaling in plants. J. Biol. Chem. **295**:7710–7725.

Chen, L., Sun, B., Xu, L., and Liu, W. (2016). Wound signaling: the missing link in plant regeneration. Plant Signal. Behav. **11**, e1238548.

Dolgikh, V.A., Pukhovaya, E.M., and Zemlyanskaya, E.V. (2019). Shaping ethylene response: the role of EIN3/EIL1 transcription factors. Front. Plant Sci. **10**:1030.

Fan, M., Xu, C., Xu, K., and Hu, Y. (2012). LATERAL ORGAN BOUNDARIES DOMAIN transcription factors direct callus formation in *Arabidopsis* regeneration. Cell Res. **22**:1169–1180.

Ferreira, P.C., Hemerly, A.S., Engler, J.D., van Montagu, M., Engler, G., and Inzé, D. (1994). Developmental expression of the *Arabidopsis* cyclin gene *cyc1At*. Plant Cell **6**:1763–1774.

Franco-Zorrilla, J.M., Valli, A., Todesco, M., Mateos, I., Puga, M.I., Rubio-Somoza, I., Leyva, A., Weigel, D., García, J.A., and Paz-Ares, J. (2007). Target mimicry provides a new mechanism for regulation of microRNA activity. Nat. Genet. **39**:1033–1037.

Friml, J., Vieten, A., Sauer, M., Weijers, D., Schwarz, H., Hamann, T., Offringa, R., and Jürgens, G. (2003). Efflux-dependent auxin gradients establish the apical-basal axis of *Arabidopsis*. Nature **426**:147–153.

Geldner, N., Friml, J., Stierhof, Y.D., Jürgens, G., and Palme, K. (2001). Auxin transport inhibitors block PIN1 cycling and vesicle trafficking. Nature **413**:425–428.

Guzmán, P., and Ecker, J.R. (1990). Exploiting the triple response of *Arabidopsis* to identify ethylene-related mutants. Plant Cell **2**:513–523.

Hernández-Coronado, M., Dias Araujo, P.C., Ip, P.L., Nunes, C.O., Rahni, R., Wudick, M.M., Lizzio, M.A., Feijó, J.A., and Birnbaum, K.D. (2022). Plant glutamate receptors mediate a bet-hedging strategy between regeneration and defense. Dev. Cell **57**:451–465.e6.

Ikeuchi, M., Iwase, A., Rymen, B., Lambolez, A., Kojima, M., Takebayashi, Y., Heyman, J., Watanabe, S., Seo, M., De Veylder, L., et al. (2017). Wounding triggers callus formation via dynamic hormonal and transcriptional changes. Plant Physiol. **175**:1158–1174.

Ikeuchi, M., Favero, D.S., Sakamoto, Y., Iwase, A., Coleman, D., Rymen, B., and Sugimoto, K. (2019). Molecular mechanisms of plant regeneration. Annu. Rev. Plant Biol. **70**:377–406.

Iwase, A., Mitsuda, N., Koyama, T., Hiratsu, K., Kojima, M., Arai, T., Inoue, Y., Seki, M., Sakakibara, H., Sugimoto, K., and Ohme-Takagi, M. (2011). The AP2/ERF transcription factor WIND1 controls cell dedifferentiation in *Arabidopsis*. Curr. Biol. **21**:508–514.

Jeong, S.W., Das, P.K., Jeoung, S.C., Song, J.Y., Lee, H.K., Kim, Y.K., Kim, W.j., Park, Y.I., Yoo, S.D., Choi, S.B., et al. (2010). Ethylene suppression of sugar-induced anthocyanin pigmentation in *Arabidopsis*. Plant Physiol. **154**:1514–1531.

Ju, C., Yoon, G.M., Shemansky, J.M., Lin, D.Y., Ying, Z.I., Chang, J., Garrett, W.M., Kessenbrock, M., Groth, G., Tucker, M.L., et al. (2012). CTR1 phosphorylates the central regulator EIN2 to control ethylene hormone signaling from the ER membrane to the nucleus in *Arabidopsis*. Proc. Natl. Acad. Sci. USA **109**:19486–19491.

Jung, J.H., Park, J.H., Lee, S., To, T.K., Kim, J.M., Seki, M., and Park, C.M. (2013). The cold signaling attenuator HIGH EXPRESSION OF OSMOTICALLY RESPONSIVE GENE1 activates FLOWERING LOCUS C transcription via chromatin remodeling under short-term cold stress in *Arabidopsis*. Plant Cell **25**:4378–4390.

Kieber, J.J., Rothenberg, M., Roman, G., Feldmann, K.A., and Ecker, J.R. (1993). CTR1, a negative regulator of the ethylene response pathway in *Arabidopsis*, encodes a member of the Raf family of protein kinases. Cell **72**:427–441.

Kim, H.J., Hong, S.H., Kim, Y.W., Lee, I.H., Jun, J.H., Phee, B.K., Rupak, T., Jeong, H., Lee, Y., Hong, B.S., et al. (2014). Gene regulatory cascade of senescence-associated NAC transcription factors activated by ETHYLENE-INSENSITIVE2-mediated leaf senescence signalling in *Arabidopsis*. J. Exp. Bot. **65**:4023–4036.

Kim, J.Y., Lee, H.J., Kim, J.A., and Jeong, M.J. (2021). Sound waves promote *Arabidopsis* thaliana root growth by regulating root phytohormone content. Int. J. Mol. Sci. **22**:5739.

Laplaze, L., Parizot, B., Baker, A., Ricaud, L., Martinière, A., Auguy, F., Franche, C., Nussaume, L., Bogusz, D., and Haseloff, J. (2005). GAL4-GFP enhancer trap lines for genetic manipulation of lateral root development in *Arabidopsis thaliana*. J. Exp. Bot. **56**:2433–2442.

Lee, H.J., Park, J.S., Shin, S.Y., Kim, S.G., Lee, G., Kim, H.S., Jeon, J.H., and Cho, H.S. (2020). Submergence deactivates wound-induced plant defence against herbivores. Commun. Biol. **3**:651.

Lee, K., Park, O.S., and Seo, P.J. (2018). JMJ30-mediated demethylation of H3K9me3 drives tissue identity changes to promote callus formation in *Arabidopsis*. Plant J. **95**:961–975.

Lee, K., and Seo, P.J. (2018). Dynamic epigenetic changes during plant regeneration. Trends Plant Sci. **23**:235–247.

Lee, Y.H., and Hong, J.K. (2015). Differential defence responses of susceptible and resistant kimchi cabbage cultivars to anthracnose, black spot and black rot diseases. Plant Pathol. **64**:406–415.

Li, W., Ma, M., Feng, Y., Li, H., Wang, Y., Ma, Y., Li, M., An, F., and Guo, H. (2015). EIN2-directed translational regulation of ethylene signaling in *Arabidopsis*. Cell **163**:670–683.

Liu, J., Sheng, L., Xu, Y., Li, J., Yang, Z., Huang, H., and Xu, L. (2014). WOX11 and 12 are involved in the first-step cell fate transition during *de novo* root organogenesis in *Arabidopsis*. Plant Cell **26**:1081–1093.

Liu, Z., Li, J., Wang, L., Li, Q., Lu, Q., Yu, Y., Li, S., Bai, M.Y., Hu, Y., and Xiang, F. (2016). Repression of callus initiation by the miRNA-directed interaction of auxin-cytokinin in *Arabidopsis thaliana*. Plant J. **87**:391–402.

Merchante, C., Brumos, J., Yun, J., Hu, Q., Spencer, K.R., Enríquez, P., Binder, B.M., Heber, S., Stepanova, A.N., and Alonso, J.M. (2015). Gene-specific translation regulation mediated by the hormone-signaling molecule EIN2. Cell **163**:684–697.

Mithöfer, A., and Boland, W. (2012). Plant defense against herbivores: chemical aspects. Annu. Rev. Plant Biol. **63**:431–450.

Mousavi, S.A.R., Chauvin, A., Pascaud, F., Kellenberger, S., and Farmer, E.E. (2013). GLUTAMATE RECEPTOR-LIKE genes mediate leaf-to-leaf wound signaling. Nature **500**:422–426.

Navarro, L., Dunoyer, P., Jay, F., Arnold, B., Dharmasiri, N., Estelle, M., Voinnet, O., and Jones, J.D.G. (2006). A plant miRNA contributes to antibacterial resistance by repressing auxin signaling. Science **312**:436–439.

Parry, G., Calderon-Villalobos, L.I., Prigge, M., Peret, B., Dharmasiri, S., Itoh, H., Lechner, E., Gray, W.M., Bennett, M., and Estelle, M. (2009). Complex regulation of the TIR1/AFB family of auxin receptors. Proc. Natl. Acad. Sci. USA **106**:22540–22545.

Radhakrishnan, D., Kareem, A., Durgaprasad, K., Sreeraj, E., Sugimoto, K., and Prasad, K. (2018). Shoot regeneration: a journey from acquisition of competence to completion. Curr. Opin. Plant Biol. **41**:23–31.

Ramachandran, V., and Chen, X. (2008). Degradation of microRNAs by a family of exoribonucleases in *Arabidopsis*. Science **321**:1490–1492.

Rodríguez, F.I., Esch, J.J., Hall, A.E., Binder, B.M., Schaller, G.E., and Bleecker, A.B. (1999). A copper cofactor for the ethylene receptor ETR1 from *Arabidopsis*. Science **283**:996–998.

Ruegger, M., Dewey, E., Gray, W.M., Hobbie, L., Turner, J., and Estelle, M. (1998). The TIR1 protein of *Arabidopsis* functions in auxin response and is related to human SKP2 and yeast grr1p. Genes Dev. **12**:198–207.

Sarkar, A.K., Luijten, M., Miyashima, S., Lenhard, M., Hashimoto, T., Nakajima, K., Scheres, B., Heidstra, R., and Laux, T. (2007). Conserved factors regulate signalling in *Arabidopsis thaliana* shoot and root stem cell organizers. Nature **446**:811–814.

Sasidharan, R., and Voesenek, L.A.C.J. (2015). Ethylene-mediated acclimations to flooding stress. Plant Physiol. **169**:3–12.

Schaller, G.E., and Bleecker, A.B. (1995). Ethylene-binding sites generated in yeast expressing the *Arabidopsis ETR1* gene. Science **270**:1809–1811.

Shin, J., Bae, S., and Seo, P.J. (2020). *De novo* shoot organogenesis during plant regeneration. J. Exp. Bot. **71**:63–72.

Stepanova, A.N., and Alonso, J.M. (2009). Ethylene signaling and response: where different regulatory modules meet. Curr. Opin. Plant Biol. **12**:548–555.

Sugimoto, K., Jiao, Y., and Meyerowitz, E.M. (2010). *Arabidopsis* regeneration from multiple tissues occurs via a root development pathway. Dev. Cell **18**:463–471.

Tadeo, F.R., Tudela, D., and Primo-Millo, E. (1995). 1-Aminocyclopropane-1-carboxylic acid-induced ethylene stimulates callus formation by cell enlargement in the cambial region of internodal explants of *Citrus*. Plant Sci. **110**:113–119.

Vain, P., Flament, P., and Soudain, P. (1990). Role of ethylene in embryogenie callus initiation and regeneration in *Zea mays* L. J. Plant Physiol. **135**:537–540.

Varkonyi-Gasic, E., Wu, R., Wood, M., Walton, E.F., and Hellens, R.P. (2007). Protocol: a highly sensitive RT-PCR method for detection and quantification of microRNAs. Plant Methods **3**:12.

Wang, J.W., Wang, L.J., Mao, Y.B., Cai, W.J., Xue, H.W., and Chen, X.Y. (2005). Control of root cap formation by MicroRNA-targeted auxin response factors in *Arabidopsis*. Plant Cell **17**:2204–2216.

Wang, L., Liu, Z., Qiao, M., and Xiang, F. (2018). miR393 inhibits *in vitro* shoot regeneration in *Arabidopsis thaliana* via repressing TIR1. Plant Sci. **266**:1–8.

Wang, R., Zhang, Y., Kieffer, M., Yu, H., Kepinski, S., and Estelle, M. (2016). HSP90 regulates temperature-dependent seedling growth in *Arabidopsis* by stabilizing the auxin co-receptor F-box protein TIR1. Nat. Commun. **7**, 11677.

Xu, C., Cao, H., Zhang, Q., Wang, H., Xin, W., Xu, E., Zhang, S., Yu, R., Yu, D., and Hu, Y. (2018a). Control of auxin-induced callus formation by bZIP59–LBD complex in *Arabidopsis* regeneration. Nat. Plants **4**:108–115.

Xu, C., Zhang, Y., Huang, Z., Yao, P., Li, Y., and Kang, X. (2018b). Impact of the leaf cut callus development stages of Populus on the tetraploid production rate by colchicine treatment. J. Plant Growth Regul. **37**:635–644.

Zhang, G., Zhao, F., Chen, L., Pan, Y., Sun, L., Bao, N., Zhang, T., Cui, C.X., Qiu, Z., Zhang, Y., et al. (2019). Jasmonate-mediated wound signalling promotes plant regeneration. Nat. Plants **5**:491–497.

Zhang, X., Henriques, R., Lin, S.S., Niu, Q.W., and Chua, N.H. (2006). Agrobacterium-mediated transformation of *Arabidopsis thaliana* using the floral dip method. Nat. Protoc. **1**:641–646.

Zhao, Y., Yu, Y., Zhai, J., Ramachandran, V., Dinh, T.T., Meyers, B.C., Mo, B., and Chen, X. (2012). The *Arabidopsis* nucleotidyl transferase HESO1 uridylates unmethylated small RNAs to trigger their degradation. Curr. Biol. **22**:689–694.